



저작자표시-비영리-변경금지 2.0 대한민국

이용자는 아래의 조건을 따르는 경우에 한하여 자유롭게

- 이 저작물을 복제, 배포, 전송, 전시, 공연 및 방송할 수 있습니다.

다음과 같은 조건을 따라야 합니다:



저작자표시. 귀하는 원저작자를 표시하여야 합니다.



비영리. 귀하는 이 저작물을 영리 목적으로 이용할 수 없습니다.



변경금지. 귀하는 이 저작물을 개작, 변형 또는 가공할 수 없습니다.

- 귀하는, 이 저작물의 재이용이나 배포의 경우, 이 저작물에 적용된 이용허락조건을 명확하게 나타내어야 합니다.
- 저작권자로부터 별도의 허가를 받으면 이러한 조건들은 적용되지 않습니다.

저작권법에 따른 이용자의 권리는 위의 내용에 의하여 영향을 받지 않습니다.

이것은 [이용허락규약\(Legal Code\)](#)을 이해하기 쉽게 요약한 것입니다.

[Disclaimer](#)

Thesis for the Degree of Master of Technology

**A novel optical thermometry based on the  
energy transfer from charge transfer band to  
 $\text{Eu}^{3+}$ - $\text{Dy}^{3+}$  ions in  $\text{SrWO}_4$**

by

Jing Wang

Interdisciplinary Program of Biomedical, Mechanical &  
Electrical Engineering

The Graduate School

Pukyong National University

August 2017

**A novel optical thermometry based on the  
energy transfer from charge transfer band to  
 $\text{Eu}^{3+}$ - $\text{Dy}^{3+}$  ions in  $\text{SrWO}_4$**

에너지 전달을 이용한 새로운  $\text{SrWO}_4:\text{Eu}^{3+}:\text{Dy}^{3+}$

광학온도계 연구

Advisor: Prof. Hyo Jin Seo

By

Jing Wang

A thesis submitted in partial fulfillment of the requirements  
for the degree of

Master of Engineering

in Interdisciplinary Program of Biomedical, Mechanical &  
Electrical Engineering, The Graduate School,  
Pukyong National University

August 2017

**A novel optical thermometry based on the  
energy transfer from charge transfer band to  
Eu<sup>3+</sup>-Dy<sup>3+</sup> ions in SrWO<sub>4</sub>**

A dissertation

by

Jing Wang

Approved by:

(Chairman: Professor Cheol Woo Park)

(Member: Ph.D. Kyoung Hyuk Jang)

(Member: Professor Hyo Jin Seo)

August 2017

## Contents

|   |    |
|---|----|
| Abstract.....   | ii |
| 1. Introduction .....   | 1  |
| 2. Background and methods of optical temperature sensing.....                                 | 3  |
| 2.1. Temperature dependent nonradiative processes of lanthanide luminescence .....            | 4  |
| 2.2. Methods of optical temperature sensing.....  | 9  |
| 3. Sample preparation and spectroscopic measurement.....                                      | 11 |
| 3.1. Sample preparation .....   | 11 |
| 3.2. Characterization.....  | 12 |
| 4. Results and discussion.....  | 13 |
| 4.1. Structure and morphology .....   | 13 |
| 4.1.1. X-ray diffraction patterns of SrWO <sub>4</sub> .....                                  | 13 |
| 4.1.2. Morphology and composition.....  | 17 |
| 4.2. Luminescence properties of SrWO <sub>4</sub> : Eu <sup>3+</sup> , Dy <sup>3+</sup> ..... | 20 |
| 4.2.1. Excitation and emission spectra.....   | 20 |
| 4.2.2. Optical temperature sensing performance .....  | 27 |
| 5. Conclusions .....  | 37 |
| Acknowledgements .....  | 38 |
| References .....  | 39 |

# **A novel optical thermometry based on the energy transfer from charge transfer band to $\text{Eu}^{3+}$ - $\text{Dy}^{3+}$ ions in $\text{SrWO}_4$**

Jing Wang

Interdisciplinary Program of Biomedical, Mechanical & Electrical Engineering

Pukyong National University

## **Abstract**

Optical thermometry based on the up-conversion intensity ratio of thermally coupled levels of rare earth ions has been widely studied to achieve an inaccessible temperature measurement in submicron scale. In this work, a novel optical temperature sensing strategy based on the energy transfer from charge transfer bands of W-O and Eu-O to  $\text{Eu}^{3+}$ - $\text{Dy}^{3+}$  ions is proposed. A series of  $\text{Eu}^{3+}/\text{Dy}^{3+}$  co-doped  $\text{SrWO}_4$  is synthesized by the conventional high-temperature solid-state method. It is found that the emission spectra, emission intensity ratio of  $\text{Dy}^{3+}$  (572 nm) and  $\text{Eu}^{3+}$  (615 nm), fluorescence color, lifetime decay curves of  $\text{Dy}^{3+}$  (572 nm) and  $\text{Eu}^{3+}$  (615 nm), and relative and absolute sensitivities of  $\text{Eu}^{3+}/\text{Dy}^{3+}$  co-doped  $\text{SrWO}_4$  are temperature dependent under the 266 nm excitation in the temperature range from 11 K to 529 K. The emission intensity ratio of  $\text{Dy}^{3+}$  (572 nm) and  $\text{Eu}^{3+}$  (615 nm) ions exhibits exponentially relation to

the temperature due to the different energy transfer from the charge transfer bands to  $\text{Dy}^{3+}$  and  $\text{Eu}^{3+}$  ions. In this host, the maximum relative sensitivity  $S_r$  can be reached as high as  $1.71\% \text{ K}^{-1}$ , being much higher than those previously reported material. It opens a new route to obtain optical thermometry with high sensitivity through using down-conversion fluorescence under ultraviolet excitation.



# 1. Introduction

Recently, white light emitting diode (LED) technology has attracted much attention in the solid-state lighting industry, due to the advantages of white LEDs including power saving, long lifetime, and environmental benefit<sup>1-3</sup>. Single-phase luminescent materials that can directly emit white light under UV excitation have been explored in oxyfluoride glass and oxides matrices<sup>4,5</sup>. The  $\text{Eu}^{3+}$  and  $\text{Dy}^{3+}$  ions were chosen as the red, green, and blue emitting activator centers through the transitions  ${}^5\text{D}_0 \rightarrow {}^7\text{F}_2$  ( $\text{Eu}^{3+}$ ),  ${}^4\text{F}_{9/2} \rightarrow {}^6\text{H}_{13/2}$  ( $\text{Dy}^{3+}$ ) and  ${}^4\text{F}_{9/2} \rightarrow {}^6\text{H}_{15/2}$  ( $\text{Dy}^{3+}$ ) under UV excitation<sup>6-8</sup>. For examples, Das and co-authors reported the controllable white light emission from  $\text{Dy}^{3+}$ - $\text{Eu}^{3+}$  co-doped  $\text{KCaBO}_3$  phosphor<sup>6</sup>. Laguna reported the shape controlled white light emission from  $\text{Dy}^{3+}$ - $\text{Eu}^{3+}$  co-doped  $\text{CaMoO}_4$  microarchitectures<sup>7</sup>. Hirai obtained the white light emission from  $\text{Dy}^{3+}$ - $\text{Eu}^{3+}$  co-doped  $\text{Sr}_2\text{CeO}_4$ <sup>8</sup>. In these works, the white light emission was controlled by changing doping concentration and host types.

It was reported that the temperature was a key parameter to adjust the emission intensity, the fluorescence intensity ratio, and emission color<sup>9-12</sup>. Berry found that the lifetime of  ${}^5\text{D}_0$  of  $\text{Eu}^{3+}$  ion was temperature dependent in Europium Tris(2,2,6,6-tetramethyl-3,5-heptanedionato)<sup>9</sup>. Morgan observed that the homogeneous linewidth of the  ${}^5\text{D}_0 \rightarrow {}^7\text{F}_0$  transition of  $\text{Eu}^{3+}$  was dependent on temperature in amorphous hosts<sup>10</sup>. Eckert observed that the phosphorescence decay lifetime of the  $\text{Dy}^{3+}$ -transitions in  $\text{Dy}^{3+}:\text{Al}_2\text{O}_3$  showed strong temperature dependency in

a temperature range from 1100 to 1500 K<sup>11</sup>. Zhou reported that the emission intensity ratio of  ${}^5D_1$  to  ${}^5D_0$  of  $\text{Eu}^{3+}$ -doped transparent  $\text{MF}_2$  (M= Ba, Ca, Sr) glass ceramics increased with the temperature increase<sup>12</sup>. However, the temperature dependent optical property of  $\text{Dy}^{3+}$ - $\text{Eu}^{3+}$  co-doped materials has not been studied so far. It is necessary to explore the spectra and energy transfer of  $\text{Dy}^{3+}$ - $\text{Eu}^{3+}$  co-doped materials at high temperature.

From the published work on the spectra of  $\text{Dy}^{3+}$ - $\text{Eu}^{3+}$  co-doped materials, one can find that it had a little overlap of the emission spectrum between  ${}^5D_0 \rightarrow {}^7F_2$  ( $\text{Eu}^{3+}$ ) and  ${}^4F_{9/2} \rightarrow {}^6H_{13/2}$  ( $\text{Dy}^{3+}$ )<sup>13,14</sup>. It is necessary to find another ion to sensitize the  $\text{Dy}^{3+}$  and  $\text{Eu}^{3+}$  simultaneously. Notably, the  $\text{WO}_4^{2-}$  group was reported to have the wide absorption band in the ultraviolet range from 200 nm to 300 nm<sup>15-17</sup>. It may be a promise sensitizer to excite  $\text{Dy}^{3+}$  and  $\text{Eu}^{3+}$  simultaneously. Thus, in this work, the optical temperature property of  $\text{Eu}^{3+}/\text{Dy}^{3+}$  co-doped  $\text{SrWO}_4$  are studied under 266 nm excitation. It is observed that the fluorescence intensity ratio between  $\text{Eu}^{3+}$  and  $\text{Dy}^{3+}$  emissions are strongly dependent on the temperature at the temperature range from 11 K to 529 K. The  $\text{Eu}^{3+}/\text{Dy}^{3+}$  co-doped  $\text{SrWO}_4$  phosphors are proved as an excellent material used for optical thermometry, due to its maximum value of  $S_r$  as high as 1.71%  $\text{K}^{-1}$ .

## **2. Background and methods of optical temperature sensing**

As a significant fundamental physical quantity, temperature is used widely in industrial and scientific field, as well as human daily life. Optical thermometry is a technique using the luminescence signal to measure the temperatures. In recent years, the lanthanide ions doped phosphors were investigated widely on the temperature sensing performance due to its unique advantages in noncontact, rapid response, and high spatial resolution, which can be used in the harsh environment, for example, high-voltage power station, fast moving objects, and so on. The lanthanide ions doped phosphors can show abundant emission lines and relatively long lifetimes in wide spectral range, which can be used as temperature sensor. As the temperature of the phosphors changes, the luminescent characteristics, for instance, emission intensity, band position and width, rise and decay times, and emission intensity ratio may change.

The luminescence process can be expressed as follows. The excitation energy is absorbed by the ground state electrons, and then the electrons are pumped to the excited state. The excited electrons release the energy by photon radiation and the electrons back to ground state. The released photon energy distributes in the ultraviolet, visible and near-infrared spectral regions. The  $f-f$  transitions of each lanthanide ion exhibits specific luminescent characteristics due to the different energy levels of each ion.

## 2.1. Temperature dependent nonradiative processes of lanthanide luminescence

As is known that, the luminescence process is a combination of radiative and nonradiative processes.

The depopulation of the excited state can be expressed as

$$\frac{dN}{dt} = -(k_R + k_{NR}) \cdot N(t) \quad (2.1)$$

Where  $k_R$  and  $k_{NR}$  are the rates of radiative and nonradiative ratios, respectively;  $N(t)$  is the population of the excited state at time  $t$ . The radiative process produces the photon emission, while the nonradiative process contributes to the vibrational energy.

The radiative emission intensity can be expressed as

$$I = hvk_R N \quad (2.2)$$

Where  $hv$  is the transition energy per photon from excited state to the ground state.

The population of the excited state exhibits exponential decay with a time constant,  $\tau$ , which is called the lifetime of the excited state and can be expressed as

$$\tau = \frac{1}{k_R + k_{NR}} \quad (2.3)$$

The radiative decay time can be expressed as

$$\tau_R = \frac{1}{k_R} \quad (2.4)$$

The emission intensity can be decreased through different processes and such reductions are called ‘quenching’. When emission intensity decreases due to the increase of temperature, it can be called ‘thermal quenching’. And this is the basic phenomenon of all the principles of luminescent temperature measurement.

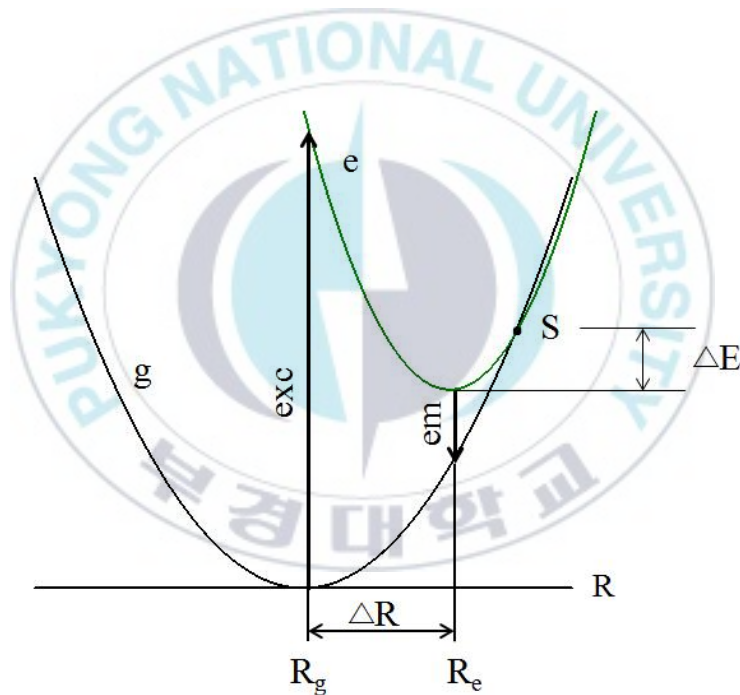


Figure 2.1. Configurational coordinate diagram illustrating the luminescence quenching at high temperature via the intersection S.

Figure 2.1 shows the configuration coordinate diagram, in which the parabolas present the total energy of the system in its ground and excited state. Absorption and emission transitions can be observed, as well as an

offset  $\Delta R$  between the parabolas of the ground and the excited state. At high temperature, the electron in the excited state can return to the ground state nonradiatively through the parabola intersection S. This temperature dependent nonradiative rate can be expressed as<sup>18</sup>

$$K_{NR}(T) = A \cdot \exp\left(\frac{-\Delta E}{k_B T}\right) \quad (2.5)$$

A is frequency constant,  $k_B$  is the Boltzmann constant,  $\Delta E$  is the energy difference between the lowest excited state and the intersection S, and the larger the  $\Delta E$  the lower the nonradiative rate. However, this process is more suitable to explain the broad band emission quenching. As for the quenching of the narrow line  $f-f$  emission, it should be explained by the multi-phonon relaxation process. The configurational coordinate diagram is shown in Figure 2.2. Two parallel parabolas that stand for the ground and excited states can be observed and will never cross. When the energy difference  $\Delta E$  is equal to or less than 4-5 times the higher vibrational frequency of the surrounding, nonradiative return to the ground state is possible by the multi-phonon relaxation process.

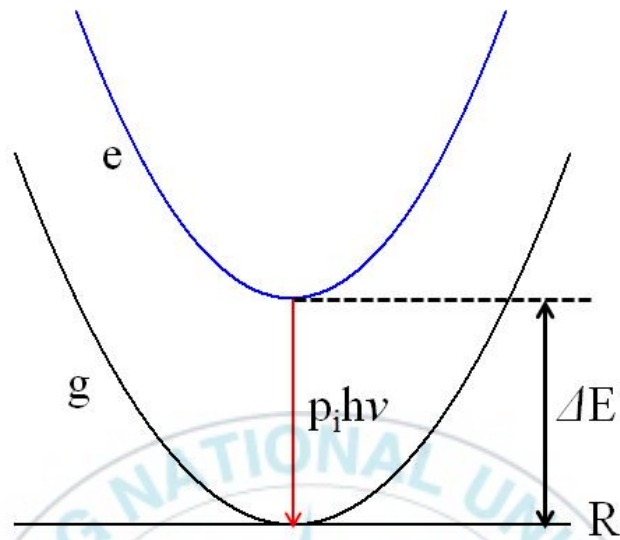


Figure 2.2. Configurational coordinate diagram illustrating the luminescence quenching via the multi-phonon relaxation process.

According to the early work<sup>19</sup>, the temperature-dependent multi-phonon transition rate can be obtained

$$K_{NR}(T) = K_{NR}(0) \left( \frac{\exp(h\nu/k_B T)}{\exp(h\nu/k_B T) - 1} \right)^{p_i} \quad (2.6)$$

$$p_i h\nu = \Delta E \quad (2.7)$$

where  $K_{NR}(0)$  is the nonradiative rate at 0 K,  $h\nu$  is the dominant phonon energy of the lattice,  $p_i$  is the number of phonons that needed in this process, and  $\Delta E$  is the energy gap from the excited level to the next lowest level. However, the higher the energy gap the lower the probability this process is.

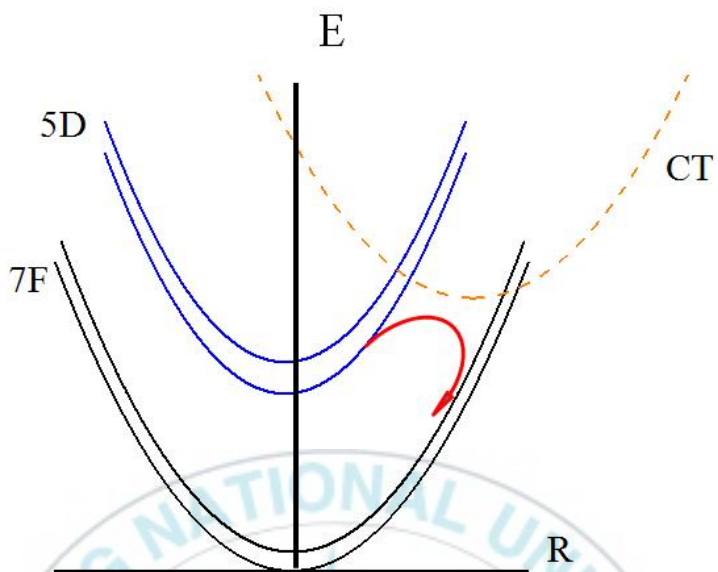


Figure 2.3. Configurational coordinate diagram illustrating the luminescence quenching via charge transfer state.

The luminescence can also be quenched by the transition through the charge transfer state to the ground levels if the charge transfer state has a large offset, for example, the  $\text{Eu}^{3+}$  ion<sup>20</sup>. The configuration coordinate diagram of this nonradiative pathway is shown in Figure 2.3.

## 2.2. Methods of optical temperature sensing

In general, the emission spectra of all the materials are temperature dependent. Several methods have been used to detect the temperature, which are expressed as following:

Emission line-width: with the increase of the temperature, the density of phonons grows, resulting the broadening of the emission band.

Line-shift: temperature induced changes, such as the energy of electronic levels, the refractive index and dilatation of the crystal lattice, may make contribute to the luminescence line-shifts.

Intensity of the emission: The emission intensity changes with the increase of temperature due to the temperature dependent nonradiative rate. Additionally, the energy transfer between ions, between ions and host may also change the emission intensity.

Ratio of emissions intensities: the ratio of emissions can be divided into two kinds of sources. One is that the emissions originate from the single emission center, and the other one is from two or more emission centers. For the single emission center, the emissions of lanthanide ions originate from two thermally coupled excited states or originate from electron transitions that end at different Stark sublevels. The latter one uses the ratio of emissions originating from two or more lanthanide ions which doped in one host.

Lifetime: the change of the excited state lifetime of lanthanide ions shows temperature dependent relationship, which is relatively small at low

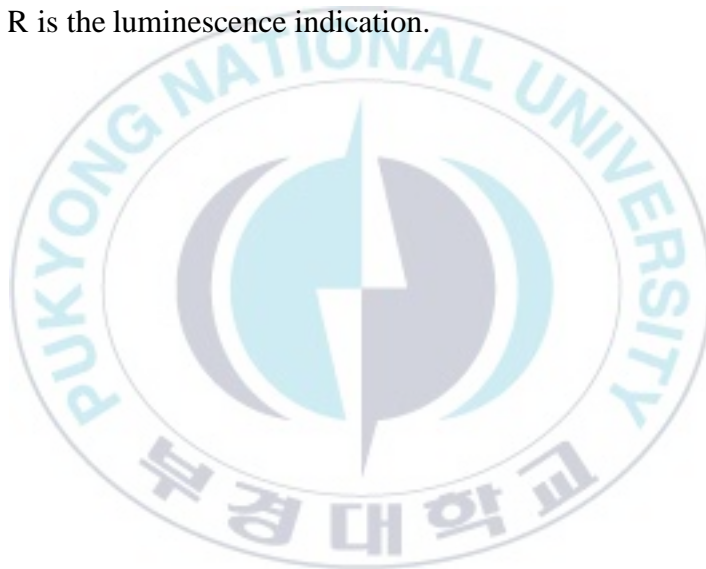
temperature while big at high temperature.

To evaluate the temperature sensing performance, the sensitivity is a key parameter. The absolute sensitivity and relative sensitivity can be defined as

$$S_a = \frac{dR}{dT} \quad (2.8)$$

$$S_r = \frac{1}{R} \frac{dR}{dT} \quad (2.9)$$

Where R is the luminescence indication.



### **3. Sample preparation and spectroscopic measurement**

#### **3.1. Sample preparation**

A series of  $\text{Eu}^{3+}/\text{Dy}^{3+}$  single doped and co-doped  $\text{SrWO}_4$  phosphors were prepared by the high-temperature solid-state method. According to the appropriate stoichiometric ratio, the starting materials,  $\text{SrCO}_3$  (Aldrich, 99.9 %),  $\text{WO}_3$  (Aldrich, 99.9 %),  $\text{Eu}_2\text{O}_3$  (Aladdin, 99.99 %), and  $\text{Dy}_2\text{O}_3$  (Aldrich, 99.99 %) were weighted and ground thoroughly in an agate mortar for 30 minutes with ethanol. Then the homogenous mixture was collected into a crucible and sintered at  $1000^\circ\text{C}$  for 4 hours. After cooling to the room temperature, the obtained white samples were ground to powder for further investigation.

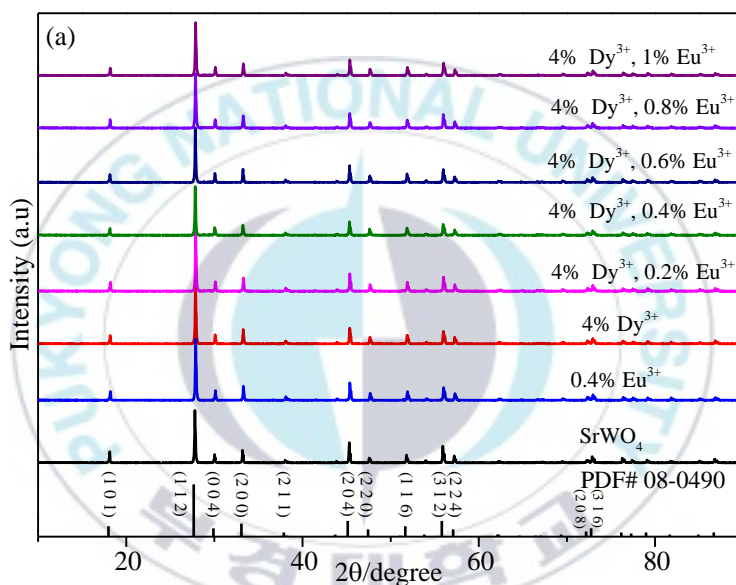
### 3.2. Characterization

In this work, The obtained products are characterized by X-ray diffraction (XRD) using a Philips X'Pert MPD (Philips, Netherlands) X-ray diffractometer at 40 kV and 30 mA. All patterns are recorded in the range of 10-90 ° with a step size of  $\Delta 2\theta = 0.02$ . The morphology, particle size and energy dispersive spectrometer (EDS) of the phosphor are characterized by scanning electron microscope (SEM) system (JSM-6490, JEOL Company). The ultraviolet-visible diffuse reflectance spectrum is recorded using a V-670 (JASCO) UV-vis spectrophotometer. The photoluminescence excitation (PLE) spectra are recorded by a Pjoton Technology International (PTI, USA) fluorimeter with a 60 W Xe-arc lamp as the excitation light source at room temperature. The photoluminescence (PL) spectra and decay lifetimes are collected by a 266 nm-pulsed Nd: YAG laser with a pulse width of 5 ns and a repetition rate of 10 Hz (Spectron Laser Sys. SL802G). The luminescence was dispersed by the 75cm monochromator (ActonResearch Corp. Pro-750, Acton, MA) and multiplied by the PMT (Hamamatsu R928, Hamamatsu Electronic Press Co., Ltd., Shizuoka, Japan).

## 4. Results and discussion

### 4.1. Structure and morphology

#### 4.1.1. X-ray diffraction patterns of SrWO<sub>4</sub>



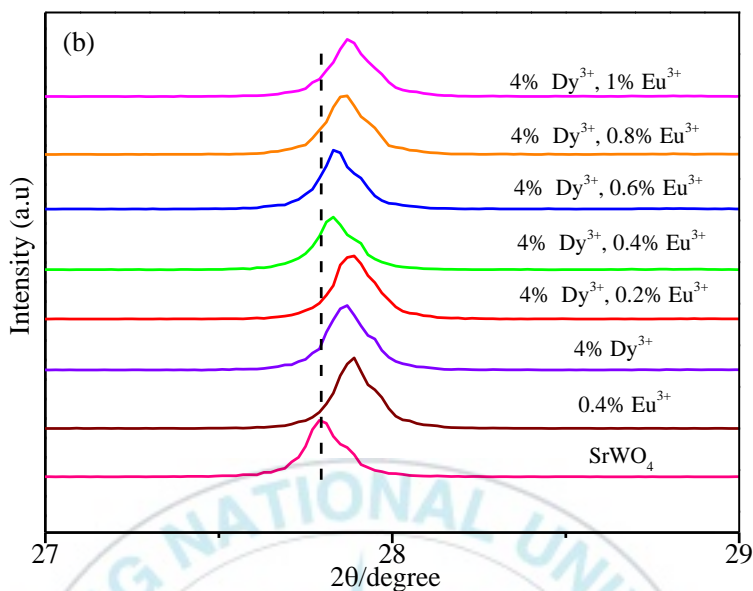


Figure 4.1 (a) XRD patterns of the as-synthesized  $\text{SrWO}_4$ ,  $\text{SrWO}_4:0.4$  mol%  $\text{Eu}^{3+}$ , and  $\text{SrWO}_4:x$   $\text{Eu}^{3+}$ , 4 mol%  $\text{Dy}^{3+}$  ( $x=0, 0.2$  mol%,  $0.4$  mol%,  $0.6$  mol%,  $0.8$  mol%,  $1$  mol%) phosphors. The standard data of tetragonal  $\text{SrWO}_4$  (PDF# 08-0490) is given as a reference; (b) Partially enlarged XRD patterns of the corresponding phosphors ( $2\theta = 27\sim 29^\circ$ ).

X-ray powder diffraction (XRD) measurements were performed in order to characterize the phase purity and the structure. XRD patterns of the  $\text{SrWO}_4$ ,  $\text{SrWO}_4:0.4$  mol%  $\text{Eu}^{3+}$ , and  $\text{SrWO}_4:x$   $\text{Eu}^{3+}$ , 4 mol%  $\text{Dy}^{3+}$  ( $x=0, 0.2$  mol%,  $0.4$  mol%,  $0.6$  mol%,  $0.8$  mol%,  $1$  mol%) samples synthesized by high-temperature solid-state reaction method are shown in Figure 4.1. The peaks of all the products can be easily indexed to tetragonal system of  $\text{SrWO}_4$ , which has an  $I41/a$  space group (PDF# 08-0490, unit cell parameters:  $a = b = 5.416 \text{ \AA}$ ,  $c = 11.95 \text{ \AA}$ ). No trace of impurity peaks can be found when  $\text{Dy}^{3+}$  and  $\text{Eu}^{3+}$  ions are introduced into the system.

Compared with the pure SrWO<sub>4</sub>, the diffraction peaks of the Eu<sup>3+</sup>, Dy<sup>3+</sup> single-doped and Eu<sup>3+</sup>/Dy<sup>3+</sup> co-doped SrWO<sub>4</sub> exhibit a slight shift toward high-angle side, due to substitution of Sr<sup>2+</sup> (1.26 Å, CN = 8) ions by smaller size Dy<sup>3+</sup> (1.03 Å, CN = 8) and Eu<sup>3+</sup> (1.07 Å, CN = 8) ions, which revealing that Dy<sup>3+</sup> and Eu<sup>3+</sup> ions have been successfully doped into the system<sup>21,22</sup>

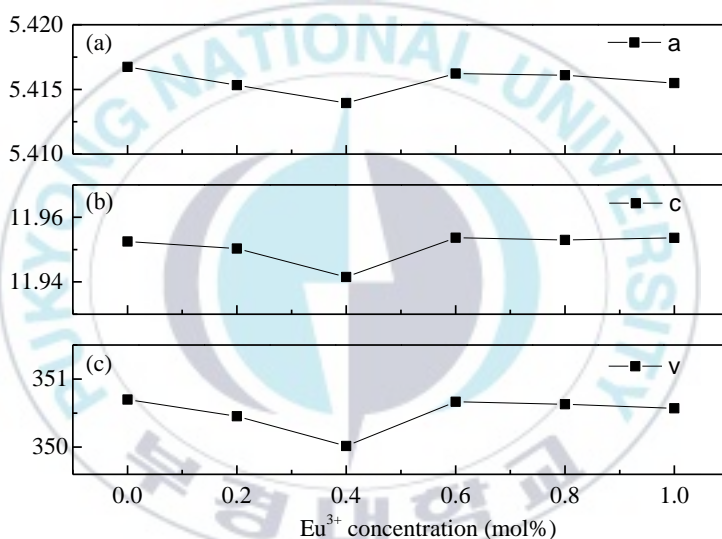


Figure 4.2 (a) Unit cell parameters of *a* (Å) and (b) *c* (Å) and (c) unit cell volume (Å<sup>3</sup>) at different Eu<sup>3+</sup> concentration in tetragonal SrWO<sub>4</sub>:*x* Eu<sup>3+</sup>, 4 mol% Dy<sup>3+</sup> (*x*=0, 0.2 mol%, 0.4 mol%, 0.6 mol%, 0.8 mol%, 1 mol%).

Figure 4.2 shows the unit cell parameters of *a* (Å) and *c* (Å) as well as unit cell volume (Å<sup>3</sup>). It can be observed that the value of lattice parameter *a* (Å) decreases firstly due to substitution of Sr<sup>2+</sup> ions by smaller size Dy<sup>3+</sup> and Eu<sup>3+</sup> ions, and then increases with the increase of

$\text{Eu}^{3+}$  concentration due to the size differences between the different valence state cations<sup>23,24</sup>. The same tendency can be observed in the values of parameter  $b$  ( $\text{\AA}$ ) and volume ( $\text{\AA}^3$ ). It reveals that  $\text{Eu}^{3+}$  and  $\text{Dy}^{3+}$  ions can be easily doped into  $\text{SrWO}_4$  lattice, and the lattice can be distorted by the doping ions.



### 4.1.2. Morphology and composition

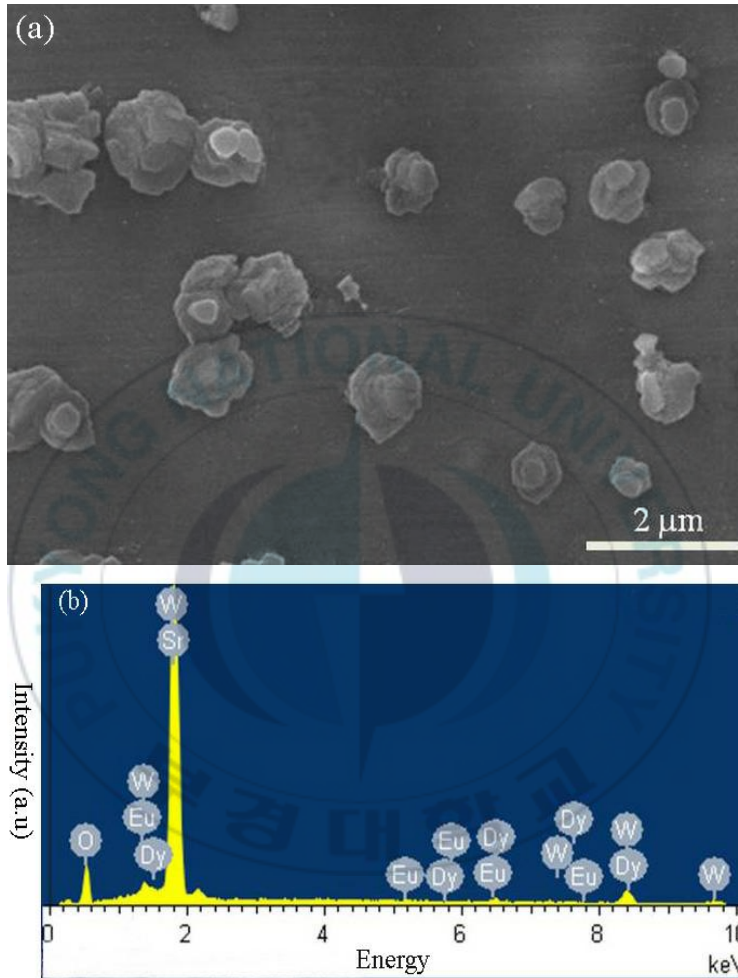


Figure 4.3 (a) SEM and (b) EDS images of the  $\text{Eu}^{3+}/\text{Dy}^{3+}$  co-doped  $\text{SrWO}_4$  phosphor.

The scanning electron microscopy (SEM) image of a representative  $\text{SrWO}_4: 0.4 \text{ mol\% Eu}^{3+}, 4 \text{ mol\% Dy}^{3+}$  sample is shown in Figure 4.3(a), exhibiting sphere-like morphology with a particle size of about 1 μm. The

energy dispersive spectrometer (EDS) spectrum (Figure 4.3(b)) confirms the presence of Sr, W, O, Eu, and Dy elements, and further providing the evidence that  $\text{Dy}^{3+}$  and  $\text{Eu}^{3+}$  ions have been successfully doped into the  $\text{SrWO}_4$  host lattice.

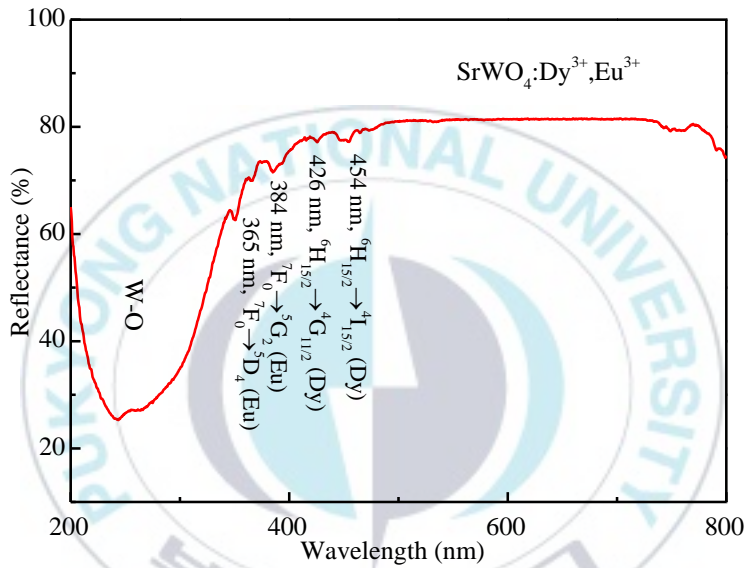


Figure 4.4 The ultraviolet-visible diffuse reflectance spectrum of the  $\text{SrWO}_4:0.4 \text{ mol\% Eu}^{3+}, 4 \text{ mol\% Dy}^{3+}$  phosphor at room temperature.

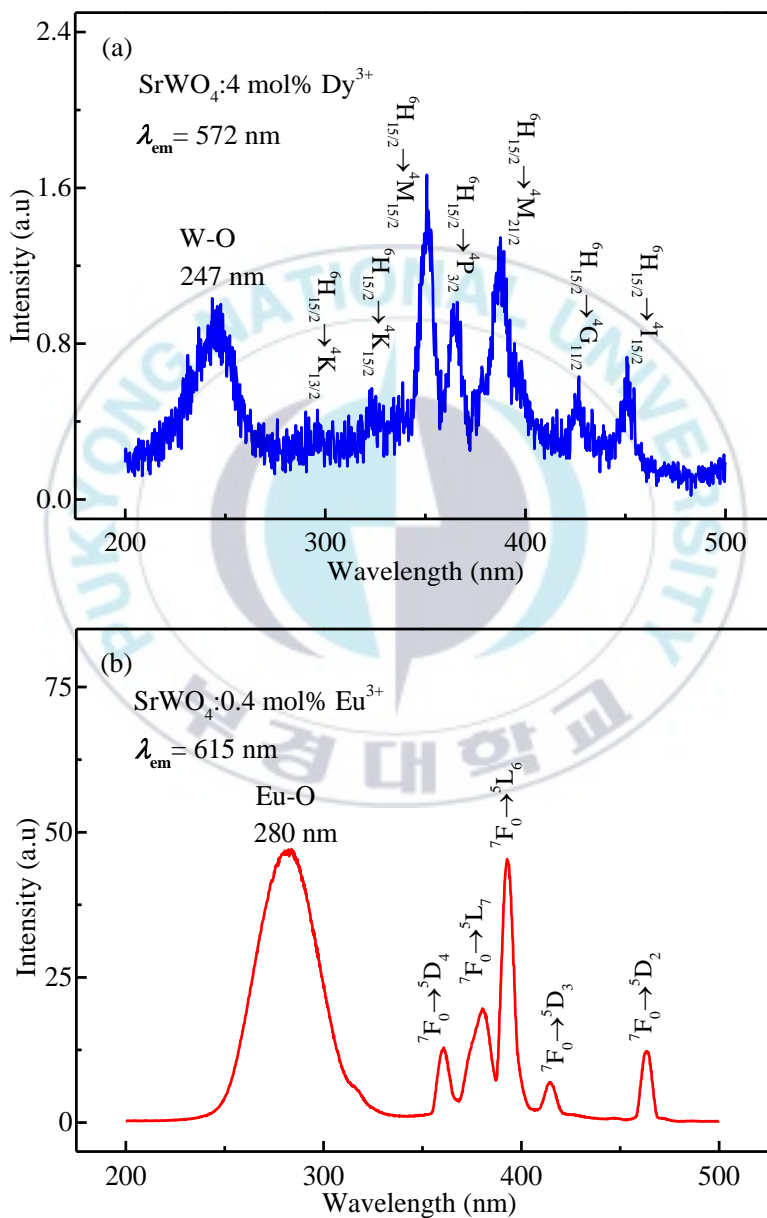
The ultraviolet-visible diffuse reflectance spectrum of the  $\text{SrWO}_4:0.4 \text{ mol\% Eu}^{3+}, 4 \text{ mol\% Dy}^{3+}$  in the range of 200-800 nm is shown in Figure 4.4. A broad band and several absorption peaks corresponding to the doped ions can be observed. The broad band is located from 200 to 350 nm, corresponding to the O-W ligand-to-metal charge transfer in the  $\text{WO}_4^{2-}$  group<sup>25,26</sup>. Four absorption peaks located at 365, 384, 426 and 454

nm can be assigned to the intra  $4f$  electronic transitions of  ${}^7F_0 \rightarrow {}^5D_4$  ( $\text{Eu}^{3+}$ ),  ${}^7F_0 \rightarrow {}^5G_2$  ( $\text{Eu}^{3+}$ ),  ${}^6H_{15/2} \rightarrow {}^4G_{11/2}$  ( $\text{Dy}^{3+}$ ), and  ${}^6H_{15/2} \rightarrow {}^4I_{15/2}$  ( $\text{Dy}^{3+}$ ), respectively.



## 4.2. Luminescence properties of SrWO<sub>4</sub>: Eu<sup>3+</sup>, Dy<sup>3+</sup>

### 4.2.1. Excitation and emission spectra



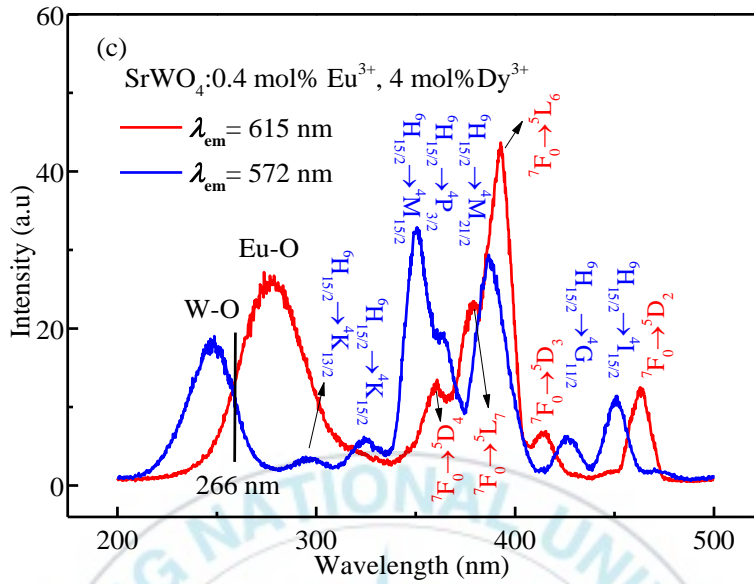
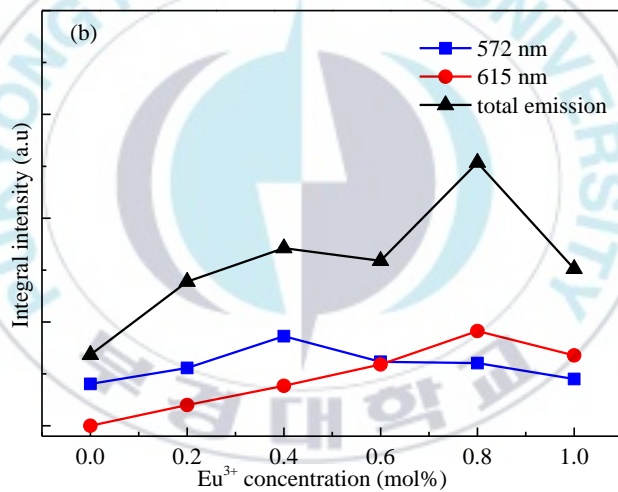
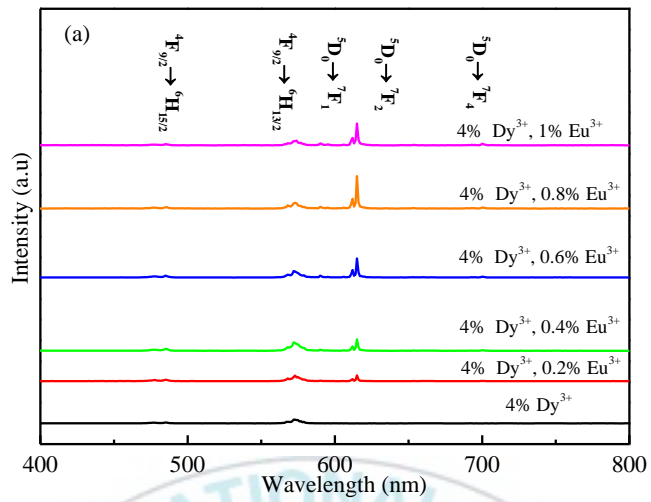


Figure 4.5 Excitation spectra of (a)  $\text{SrWO}_4:4 \text{ mol\% Dy}^{3+}$ , (b)  $\text{SrWO}_4:0.4 \text{ mol\% Eu}^{3+}$ , and (c)  $\text{SrWO}_4:0.4 \text{ mol\% Eu}^{3+}, 4 \text{ mol\% Dy}^{3+}$  phosphors at room temperature.

The PLE spectra of  $\text{SrWO}_4:4 \text{ mol\% Dy}^{3+}$ ,  $\text{SrWO}_4:0.4 \text{ mol\% Eu}^{3+}$ , and  $\text{SrWO}_4:0.4 \text{ mol\% Eu}^{3+}, 4 \text{ mol\% Dy}^{3+}$  samples are shown in Figure 4.5. The PLE spectrum of  $\text{SrWO}_4:4 \text{ mol\% Dy}^{3+}$  (Figure 4.5(a)) illustrates a broad charge transfer band centered at 247 nm from 200 to 280 nm and a series of sharp lines extended to visible region can be observed by monitoring at 572 nm. The broad band can be ascribed to a charge transfer from  $\text{WO}_4^{2-}$  group to  $\text{Dy}^{3+}$ <sup>27</sup>, and the seven sharp lines can be ascribed to  $f-f$  transitions of  $\text{Dy}^{3+}$   $4f$  configuration, which are  ${}^6\text{H}_{15/2} \rightarrow {}^4\text{K}_{13/2}$  (296 nm),  ${}^6\text{H}_{15/2} \rightarrow {}^4\text{K}_{15/2}$  (322 nm),  ${}^6\text{H}_{15/2} \rightarrow {}^4\text{M}_{15/2}$  (350 nm),  ${}^6\text{H}_{15/2} \rightarrow {}^4\text{P}_{3/2}$  (365 nm),  ${}^6\text{H}_{15/2} \rightarrow {}^4\text{M}_{21/2}$  (387 nm),  ${}^6\text{H}_{15/2} \rightarrow {}^4\text{G}_{11/2}$  (426 nm), and  ${}^6\text{H}_{15/2} \rightarrow {}^4\text{I}_{15/2}$  (450

nm), respectively<sup>28</sup>. The excitation spectrum of SrWO<sub>4</sub>: 0.4 mol% Eu<sup>3+</sup> is shown in Figure 4.5(b). Monitored at 615 nm, an intense broad band can be found in the range of 250-320 nm, which is due to Eu-O charge transfer transition<sup>29</sup>. While in the range of 200-250 nm, no obvious band can be found, indicating the energy transfer from WO<sub>4</sub><sup>2-</sup> group to Eu<sup>3+</sup> is negligible. Additionally, a series of sharp lines corresponding to the intra 4f electron transitions of Eu<sup>3+</sup> ion can also be observed, which are 360 nm (<sup>7</sup>F<sub>0</sub>→<sup>5</sup>D<sub>4</sub>), 380 nm (<sup>7</sup>F<sub>0</sub>→<sup>5</sup>L<sub>7</sub>), 393 nm (<sup>7</sup>F<sub>0</sub>→<sup>5</sup>L<sub>6</sub>), 414 nm (<sup>7</sup>F<sub>0</sub>→<sup>5</sup>D<sub>3</sub>), and 463 nm (<sup>7</sup>F<sub>0</sub>→<sup>5</sup>D<sub>2</sub>), respectively<sup>30</sup>. Figure 4.5(c) shows the excitation spectra of SrWO<sub>4</sub>:0.4 mol% Eu<sup>3+</sup>, 4 mol% Dy<sup>3+</sup> phosphors. When compared with the excitation spectrum of SrWO<sub>4</sub>:4 mol% Dy<sup>3+</sup> by monitoring at 572 nm, the position of broad band and the excitation peaks in both the spectra can be matched well with each other. Nevertheless, the excitation intensity of Dy<sup>3+</sup> is greatly enhanced when Eu<sup>3+</sup> is introduced. When monitored at 615 nm, the Eu<sup>3+</sup> excitation intensity decreases compared with the excitation spectrum of SrWO<sub>4</sub>:0.4 mol% Eu<sup>3+</sup>. This may be due to the energy transfer from Eu<sup>3+</sup> to Dy<sup>3+</sup>. The apparent overlap of charge transfer band centered at about 266 nm can also be observed. Hence, 266 nm pulsed laser is selected as the excitation light source to excite Dy<sup>3+</sup> and Eu<sup>3+</sup> ions.



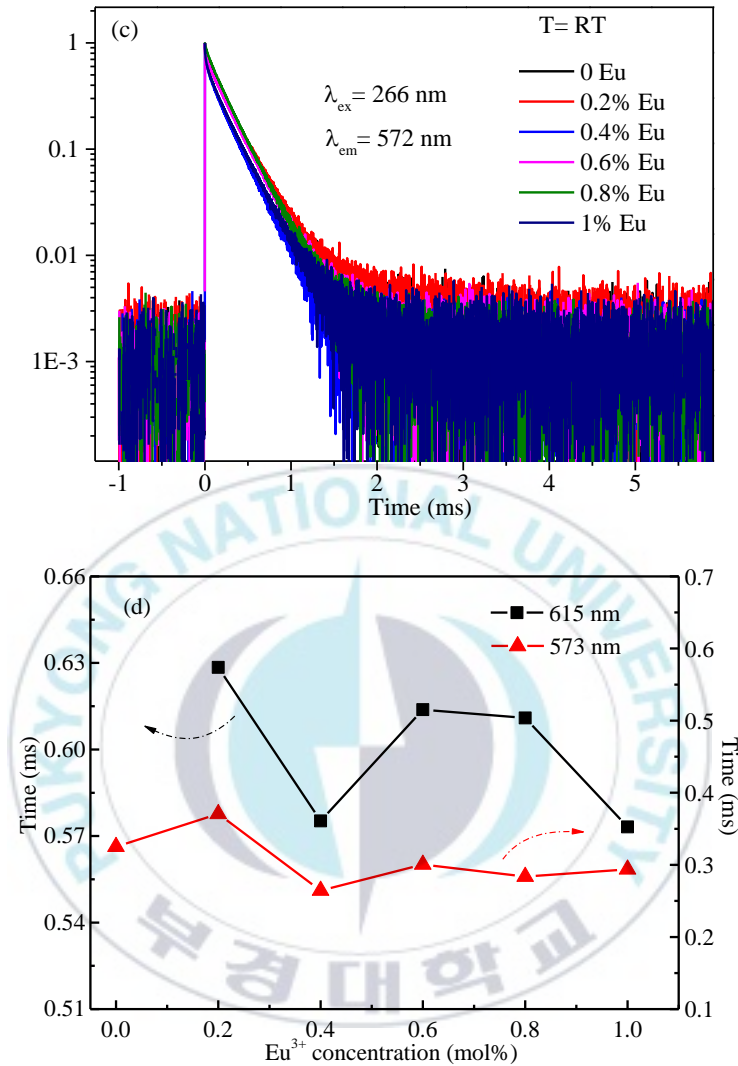


Figure 4.6 (a) PL emission spectra, (b) Integral intensity of  $\text{Dy}^{3+}$  (572 nm),  $\text{Eu}^{3+}$  (615 nm) and total emission, (c) Decay curves of  ${}^4F_{9/2}$  energy level of  $\text{Dy}^{3+}$  and (d) Calculated lifetimes of  ${}^4F_{9/2}$  and  ${}^5D_0$  energy levels of  $\text{SrWO}_4:x \text{Eu}^{3+}$ , 4 mol%  $\text{Dy}^{3+}$  ( $x=0, 0.2 \text{ mol}\%$ ,  $0.4 \text{ mol}\%$ ,  $0.6 \text{ mol}\%$ ,  $0.8 \text{ mol}\%$ ,  $1 \text{ mol}\%$ ) phosphors under 266 nm excitation at room temperature.

Figure 4.6(a) displays the emission curves of  $\text{SrWO}_4:x \text{Eu}^{3+}$ , 4 mol%

$\text{Dy}^{3+}$  ( $x=0, 0.2 \text{ mol\%}, 0.4 \text{ mol\%}, 0.6 \text{ mol\%}, 0.8 \text{ mol\%}, 1 \text{ mol\%}$ ) phosphors. The emission spectrum of the  $\text{SrWO}_4:4 \text{ mol\% Dy}^{3+}$  reveals a strong yellow (572nm) emission and a blue (485 nm) emission corresponding to the  ${}^4\text{F}_{9/2} \rightarrow {}^6\text{H}_{13/2}$  and  ${}^4\text{F}_{9/2} \rightarrow {}^6\text{H}_{15/2}$  transition of  $\text{Dy}^{3+}$  ions, respectively, under the 266 nm excitation<sup>31</sup>. Two small emission peaks located at 660 and 750 nm are also observed, due to the transitions from  ${}^4\text{F}_{9/2}$  excited state to  ${}^6\text{H}_{11/2}$  and  ${}^6\text{H}_{9/2}$  ground states. And a very weak broad band in the range of 350-550 nm corresponding to the  $\text{WO}_4^{2-}$  emission can be found. One can see that the electric dipole transition  ${}^4\text{F}_{9/2} \rightarrow {}^6\text{H}_{13/2}$  at 572 nm dominates the spectrum, which indicates that the  $\text{Dy}^{3+}$  ions are placed at the sites of non-inversion symmetry<sup>5,32</sup>. Four new emission peaks at 590, 615, 650 and 700 nm appear, due to the  $4f-4f$  transitions ( ${}^5\text{D}_0 \rightarrow {}^7\text{F}_{1,2,3,4}$ ) of  $\text{Eu}^{3+}$  ions, along with the characteristic transitions of  $\text{Dy}^{3+}$ <sup>13</sup>. The integral intensity of 572 nm and 615 nm emissions is calculated as a function of  $\text{Eu}^{3+}$  concentration as well as the total emissions, as shown in Figure 4.6(b). The emission intensity of  $\text{Eu}^{3+}$  (615 nm) increases with increase of the  $\text{Eu}^{3+}$  concentration from 0.2 mol% to 0.8 mol%, and then decreases when the concentration further increases above 0.8 mol% due to the concentration quenching effect<sup>33</sup>. The  $\text{Dy}^{3+}$  emission (572 nm) intensity increases with the increase of  $\text{Eu}^{3+}$  concentration and reaches a maximum value at  $\text{Eu}^{3+}$  concentration of 0.4 mol%, which can be ascribed to the energy transfer from  $\text{Eu}^{3+}$  to  $\text{Dy}^{3+}$ <sup>34</sup>. With the continuous increasing of  $\text{Eu}^{3+}$  concentration, the  $\text{Dy}^{3+}$  emission intensity decreases, which can be attributed to the concentration quenching effect. Focusing on the total

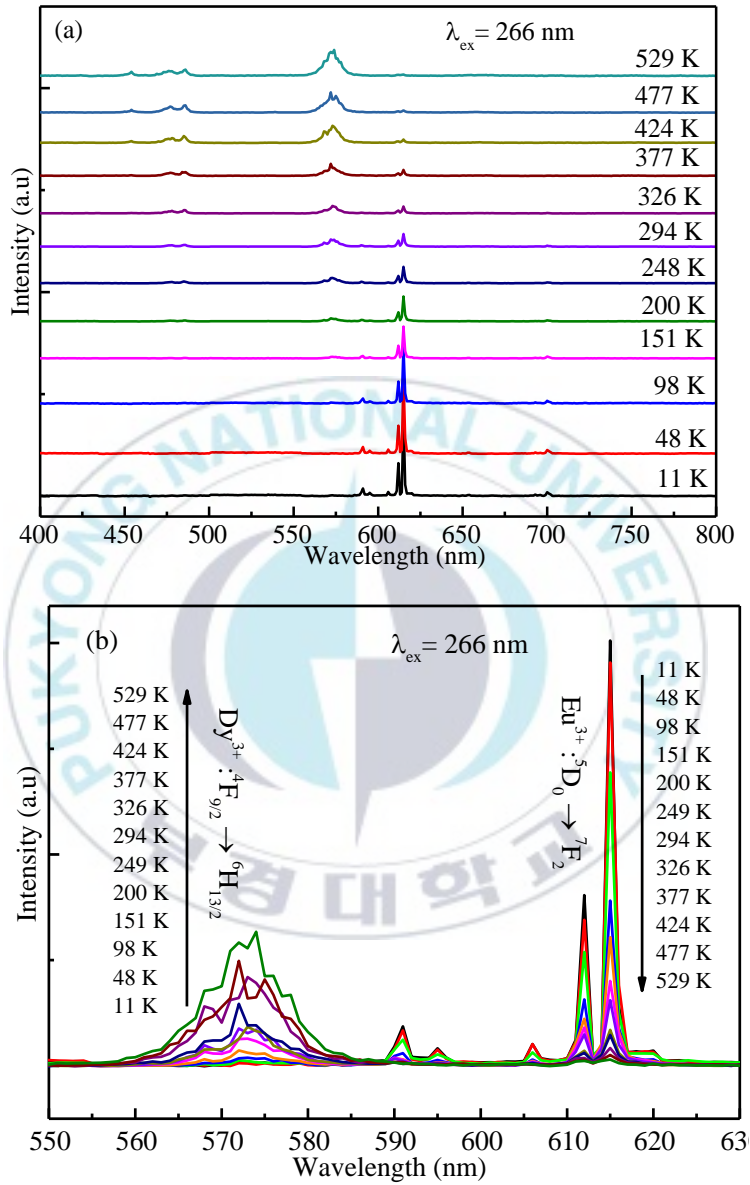
emissions intensity, when the doping concentration of  $\text{Eu}^{3+}$  reaches to 0.8 mol%, the strongest total emission intensity is obtained. Thus, the sample co-doped with 0.4 mol%  $\text{Eu}^{3+}$  and 4 mol%  $\text{Dy}^{3+}$  should be selected as the optimum doping concentration to study optical properties at different temperature.

The effective lifetimes of  ${}^4\text{F}_{9/2}$  and  ${}^5\text{D}_0$  energy levels can be expressed as<sup>35</sup>

$$\tau_{\text{eff}} = \frac{\int I(t)tdt}{\int I(t)dt} \quad (4.1)$$

where  $I(t)$  represents the emission intensity at time  $t$ . The decay curves of  $\text{Dy}^{3+}$  ( ${}^4\text{F}_{9/2}$ ) and  $\text{Eu}^{3+}$  ( ${}^5\text{D}_0$ ) ions at different  $\text{Eu}^{3+}$  concentration were recorded by monitoring at 572 nm and 615 nm, respectively. The decay curves in Figure 4.6(c) support the existence of energy transfer progress for doped and co-doped samples. The values of lifetimes of  $\text{SrWO}_4:x \text{Eu}^{3+}$ , 4 mol%  $\text{Dy}^{3+}$  ( $x=0, 0.2 \text{ mol\%}, 0.4 \text{ mol\%}, 0.6 \text{ mol\%}, 0.8 \text{ mol\%}, 1 \text{ mol\%}$ ) phosphors were calculated by using equation (1), in Figure 4.6(d). The decreasing tendency of lifetimes of both  ${}^4\text{F}_{9/2}$  and  ${}^5\text{D}_0$  energy levels can be found with the rise of  $\text{Eu}^{3+}$  concentration. The Figure 4.6(d) shows the inhomogeneous change of lifetimes of the 572 nm ( $\text{Dy}^{3+}$ ) and 615 nm ( $\text{Eu}^{3+}$ ) emissions. It means that the energy transfer from charge transfer band of W-O to  $\text{Dy}^{3+}$  and the energy transfer from charge transfer band of Eu-O to  $\text{Eu}^{3+}$  as well as energy transfer from  $\text{Eu}^{3+}$  to  $\text{Dy}^{3+}$  are different at different  $\text{Eu}^{3+}$  concentrations.

## 4.2.2. Optical temperature sensing performance



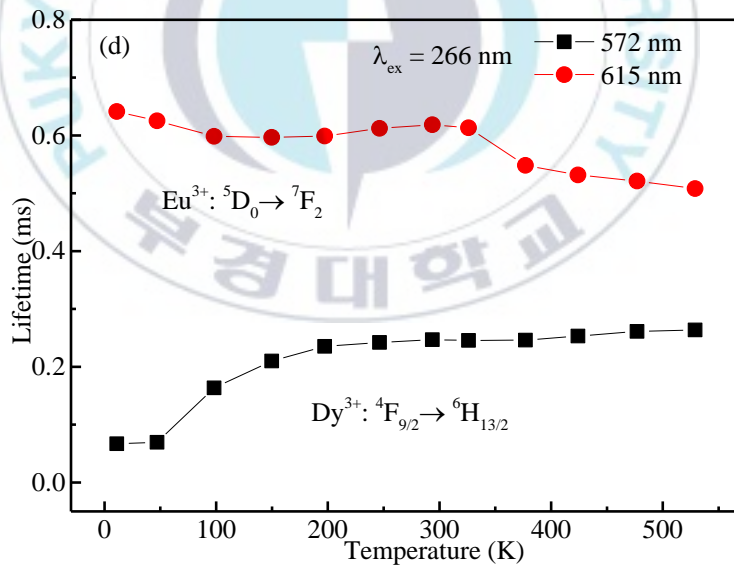
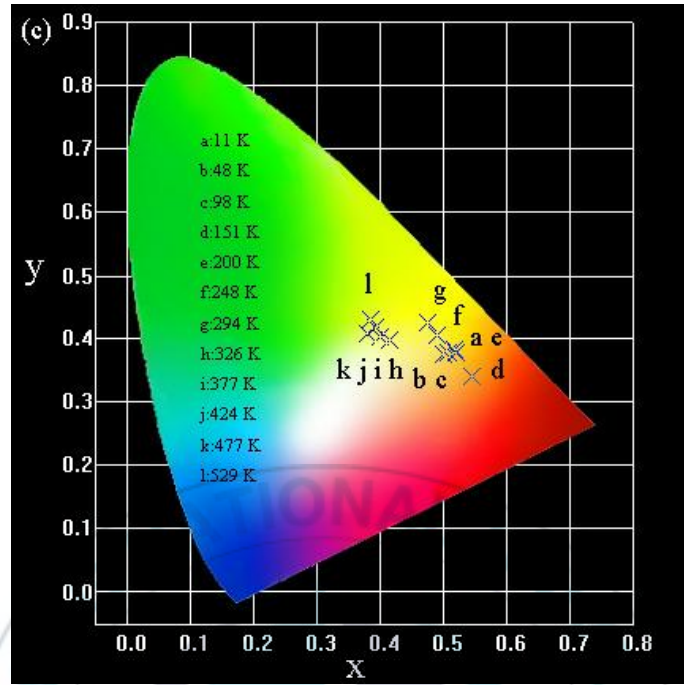


Figure 4.7 (a) PL Emission spectra, (b) Temperature-dependent spectra at 572 nm and 615 nm, (c) CIE, (d) Calculated lifetimes of <sup>4</sup>F<sub>9/2</sub> (Dy<sup>3+</sup>) and <sup>5</sup>D<sub>0</sub> (Eu<sup>3+</sup>) energy levels of Dy<sup>3+</sup> and Eu<sup>3+</sup> ions of the SrWO<sub>4</sub>:0.4 mol% Eu<sup>3+</sup>, 4 mol% Dy<sup>3+</sup> phosphor under 266 nm excitation from 11 K to 529 K.

To further study the temperature-dependent photoluminescence performance, the emission spectra of the SrWO<sub>4</sub>:0.4 mol% Eu<sup>3+</sup>, 4 mol% Dy<sup>3+</sup> samples are investigated in the temperature range from 11 K to 592 K, as shown in Figure 4.7(a). One can see that the emission intensity of Dy<sup>3+</sup> ions increases with the rise of temperature, while the emission intensity of Eu<sup>3+</sup> ions decreases. The emission bands of Dy<sup>3+</sup> ions at 572 nm (<sup>4</sup>F<sub>9/2</sub>→<sup>6</sup>H<sub>13/2</sub>) and Eu<sup>3+</sup> ions at 615 nm (<sup>5</sup>D<sub>0</sub>→<sup>7</sup>F<sub>2</sub>) were enlarged and shown in Figure 4.7(b). One can find that the intensity of 572 nm (Dy<sup>3+</sup>) increases with the temperature increase, while the intensity of 615 nm (Eu<sup>3+</sup>) decreases with the temperature increase. It means that the energy transfer from charge transfer bands to Eu<sup>3+</sup> and Dy<sup>3+</sup> ions is temperature dependent. The Commission International de L'Eclairage (CIE) diagram (Figure 4.7(c)) shows that the emission color of the SrWO<sub>4</sub>:0.4 mol% Eu<sup>3+</sup>, 4 mol% Dy<sup>3+</sup> sample can be turned from the orange-red to the yellow region with the increase of temperature from 11 K to 529 K.

In order to study the energy transfer among charge transfer bands, Eu<sup>3+</sup>, and Dy<sup>3+</sup>, the decay curves of <sup>4</sup>F<sub>9/2</sub> and <sup>5</sup>D<sub>0</sub> energy levels at different temperature were measured by monitoring at 572 nm and 615 nm, respectively, and calculated by using equation (4.1). The values of the effective lifetimes are shown in Figure 4.7(d). It can be found that the lifetimes of <sup>4</sup>F<sub>9/2</sub> energy level of Dy<sup>3+</sup> ion increase with the increase of temperature, while the lifetimes of <sup>5</sup>D<sub>0</sub> energy level of Eu<sup>3+</sup> ion decrease, demonstrating the different energy transfer rates from charge transfer bands to Dy<sup>3+</sup> and Eu<sup>3+</sup> ions<sup>36</sup>.

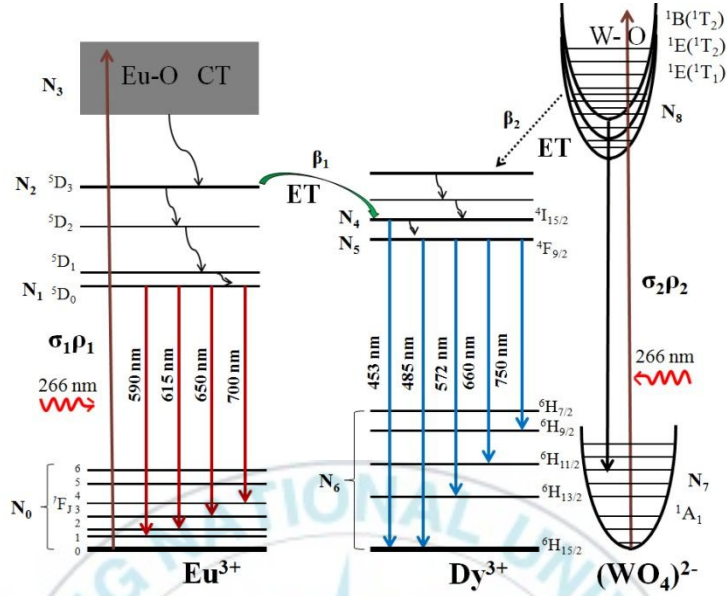


Figure 4.8 The mechanism graph of the optical temperature sensing through energy transfer from the charge transfer band to  $\text{Dy}^{3+}$  and  $\text{Eu}^{3+}$  ions under the 266 nm excitation.

To study the temperature dependence of energy transfer from charge transfer bands to  $\text{Eu}^{3+}$ - $\text{Dy}^{3+}$  ions, the dynamic balance rate-equation model for the energy transfer between charge transfer bands and  $\text{Eu}^{3+}$ - $\text{Dy}^{3+}$  ions are established in Figure 4.8. We supposed  ${}^7F_J$  ( $J=0,1,2,3,4,5,6$ ),  ${}^6H_{J/2}$  ( $J=15,13,11,9,7$ ), or  ${}^1B(^1T_2)/{}^1E(^1T_2)/{}^1E(^1T_1)$  energy levels as a same level in the case of the fixed temperature. The energy transfer between  $\text{Eu}^{3+}$  and  $\text{WO}_4^{2-}$  is neglected. The corresponding rate equations are as follows:

$$\frac{dN_1}{dt} = N_2W_{21} - N_1A_{10} \quad (4.2)$$

$$\frac{dN_2}{dt} = N_3W_{32} - \beta_1N_2N_4 - N_2W_{21} \quad (4.3)$$

$$\frac{dN_3}{dt} = \sigma_1\rho_1N_0 - N_3W_{32} \quad (4.4)$$

$$\frac{dN_5}{dt} = N_4W_{45} - N_5A_{56} \quad (4.5)$$

$$\frac{dN_8}{dt} = \sigma_2\rho_2N_7 - N_8A_{87} - \beta_2N_8N_4 \quad (4.6)$$

Where  $\sigma_1$  and  $\sigma_2$  are the cross-section of the ground state absorption of  ${}^7F_J$  and  ${}^1A_1$ ,  $\rho_1$  and  $\rho_2$  are the incident pumping power density,  $N_0$ ,  $N_1$ ,  $N_2$ ,  $N_3$ ,  $N_4$ ,  $N_5$ ,  $N_6$ ,  $N_7$ , and  $N_8$  are the population densities of the levels of  $\text{Eu}^{3+}$ ,  $\text{Dy}^{3+}$  and  $\text{WO}_4^{2-}$ , respectively.  $\beta_1$  and  $\beta_2$  correspond to the energy transfer rates from  ${}^5D_3$  and  ${}^1B({}^1T_2)/{}^1E({}^1T_2)/{}^1E({}^1T_1)$  to  ${}^4I_{15/2}$ , respectively. The terms of  $W_{ij}$  represent the nonradiative decay rates between the levels  $i$  and  $j$ ,  $A_{ij}$  is the radiative transition rates between the levels  $i$  and  $j$ .

By solving the above equations, we have

$$\frac{N_5}{N_1} \approx \frac{W_{45}A_{10}}{A_{56}W_{21}\sigma_1\rho_1N_0} \left( \frac{W_{21}}{\beta_2} + \frac{\beta_1}{\beta_2^2} \right) \quad (4.7)$$

The nonradiative relaxation possibility is proportional to<sup>37</sup>

$$W_{ij} \propto e^{-\frac{hw}{kT}} \quad (4.8)$$

The luminescence intensity of an emission band can be expressed as

$$I_{ij} = hv_i A_{ij} N_i \quad (4.9)$$

where  $hv_i$  is transition energy per photon,  $A_{ij}$  is spontaneous radiative emission probability from an  $i$  state to a  $j$  state, and  $N_i$  is the state population of the  $i$  state<sup>38</sup>.

The emission intensity ratio of  $\text{Dy}^{3+}$  (572 nm) and  $\text{Eu}^{3+}$  (615 nm) ions, defined as *FIR* ( $I_{\text{Dy}}/I_{\text{Eu}}$ ), is adopted to study the temperature-dependent

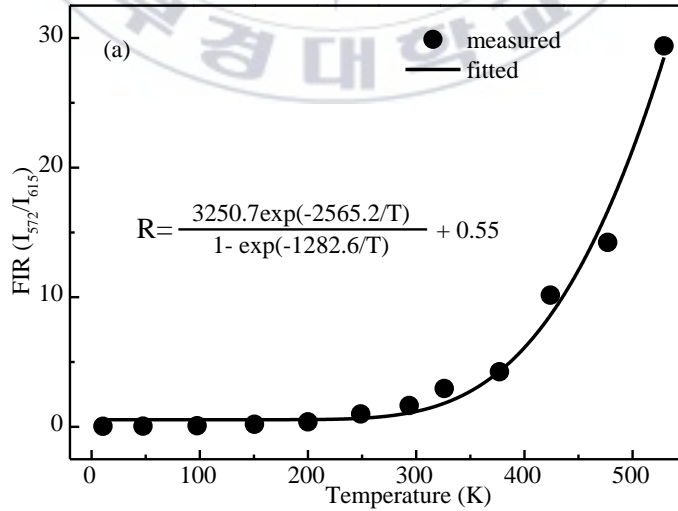
photoluminescence property. Combining with above equations, the *FIR* ( $I_{Dy}/I_{Eu}$ ) can be fitted as

$$FIR = \frac{I_{Dy}}{I_{Eu}} = \frac{A \exp(-2\hbar\omega/kT)}{1 - \exp(-\hbar\omega/kT)} + B \quad (4.10)$$

Where  $A$  is the fitting constant that depends on the experimental system and intrinsic spectroscopic parameter;  $\hbar\omega$  is the phonon energy; and  $k$  is a Boltzmann constant<sup>39</sup>. The absolute sensitivity and relative sensitivity can be defined as<sup>37</sup>

$$S_a = \frac{dR}{dT} = \frac{A\hbar\omega \exp(-3\hbar\omega/kT)}{k(1 - \exp(-\hbar\omega/kT))^2 T^2} + \frac{2A\hbar\omega \exp(-2\hbar\omega/kT)}{k(1 - \exp(-\hbar\omega/kT))T^2} \quad (4.11)$$

$$S_r = \frac{1}{R} \frac{dR}{dT} = \frac{\frac{A\hbar\omega \exp(-3\hbar\omega/kT)}{k(1 - \exp(-\hbar\omega/kT))^2 T^2} + \frac{2A\hbar\omega \exp(-2\hbar\omega/kT)}{k(1 - \exp(-\hbar\omega/kT))T^2}}{B + \frac{A \exp(-2\hbar\omega/kT)}{1 - \exp(-\hbar\omega/kT)}} \quad (4.12)$$



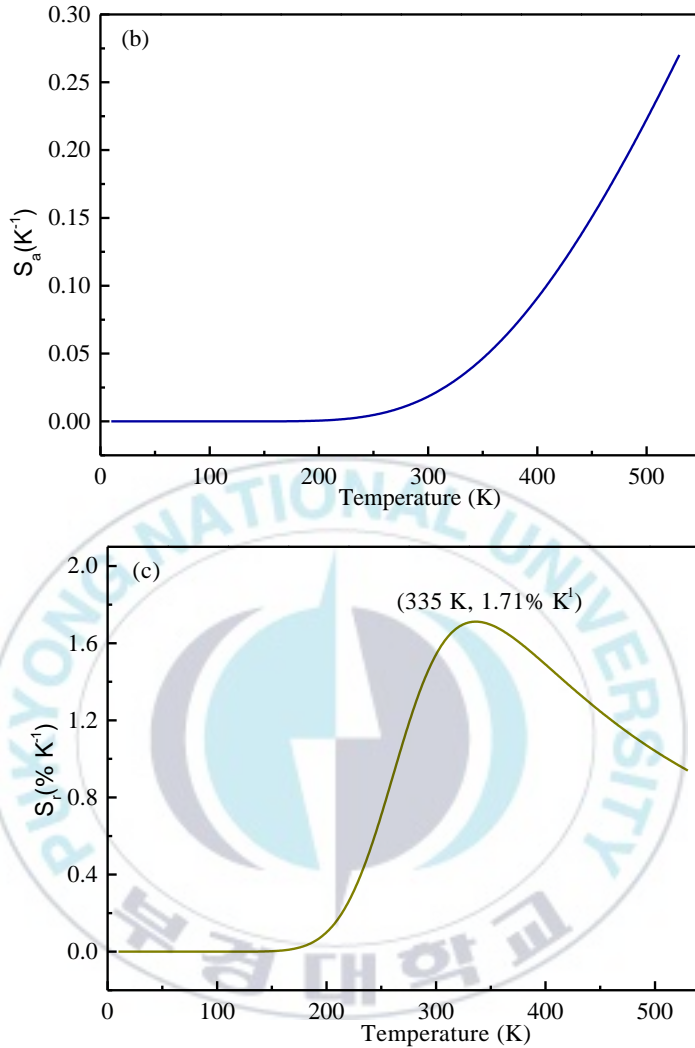
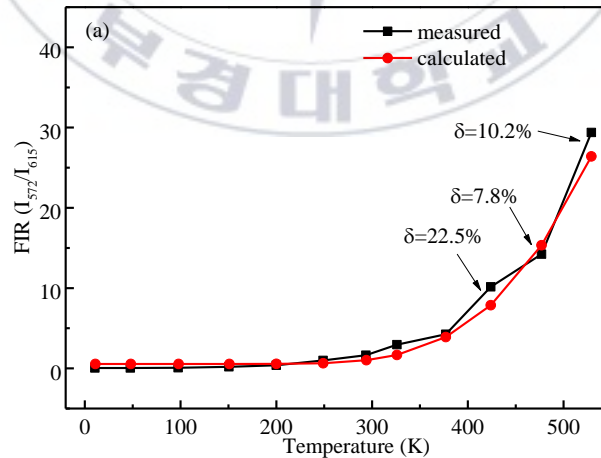


Figure 4.9 (a) Experimental measured and fitted plots of *FIR* ( $I_{572}/I_{615}$ ) versus temperature. (b) Absolute sensitivity  $S_a$  and (c) Relative sensitivity  $S_r$  versus temperature.

As displayed in Figure 4.9(a), the *FIR* data could be exponentially fitted by the equation (4.10) from 11 K to 529 K. The parameters  $A$ ,  $B$  and  $\hbar\omega$  can be determined to be 3250.7, 0.55 and  $903.8 \text{ cm}^{-1}$  for the  $\text{SrWO}_4:0.4 \text{ mol\% Eu}^{3+}, 4 \text{ mol\% Dy}^{3+}$  sample by using the fitting equation. The fitted

phonon energy of  $903.8 \text{ cm}^{-1}$  is closed to the literature reported of  $917.7 \text{ cm}^{-1}$ <sup>41</sup>. The error of the fitted phonon energy is about 1.5%. On the basis of the equation (4.11) and (4.12), the absolute sensitivity  $S_a$  and relative sensitivity  $S_r$  are calculated and shown in Figure 4.9(b,c). One can see that the absolute sensitivity is as high as  $0.27 \text{ K}^{-1}$  at 529 K. It is much higher than the literature reported<sup>42,43</sup>. For example, the absolute sensitivity in  $\text{Eu}^{3+}$  doped  $\text{Gd}_2\text{Ti}_2\text{O}_7$  phosphor was  $0.015 \text{ K}^{-1}$ <sup>44</sup>, and in  $\text{Dy}^{3+}$  doped  $\text{GdVO}_4$  phosphor was  $0.01 \text{ K}^{-1}$ <sup>45</sup>. The maximum relative sensitivity of  $1.71\% \text{ K}^{-1}$  is obtained at 335 K. It is higher than the reported phosphors,  $0.014 \text{ K}^{-1}$  in  $\text{Eu}^{3+}$  doped  $\text{CaGd}_2(\text{WO}_4)_4$  scheelite<sup>46</sup> and  $0.003 \text{ }^\circ\text{C}^{-1}$  in  $\text{Dy}^{3+}$  doped  $\text{Y}_4\text{Al}_2\text{O}_9$  phosphor<sup>47</sup>. The improvement of both the relative sensitivity and absolute sensitivity of this material may be owing to different energy transfer ratio at different temperatures, leading to a significant change in the emission intensity ratio.



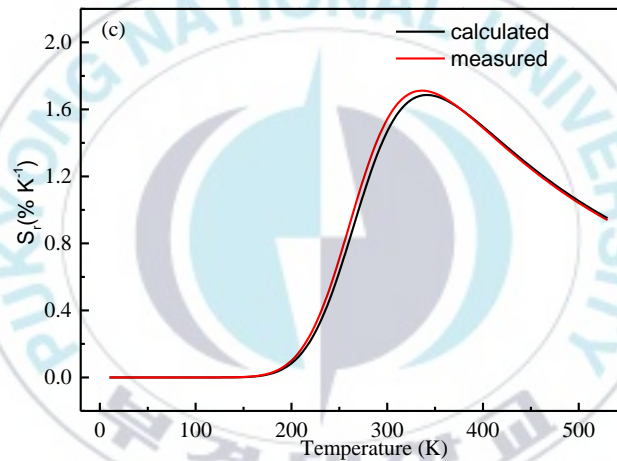
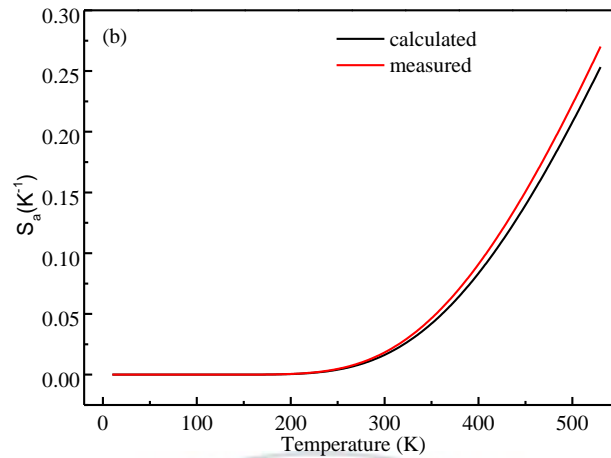


Figure 4.10 (a) Experimental measured and calculated plots of *FIR* ( $I_{572}/I_{615}$ ) versus temperature. (b) Measured and calculated absolute sensitivity  $S_a$  and (c) relative sensitivity  $S_r$  versus temperature.

The error analysis of measured and calculated *FIR* ( $I_{572}/I_{615}$ ) is shown in Figure 4.10(a). One can see that the measured and the calculated *FIR* match well at low temperature, while the error appears at high temperature more than 400 K. The error may originate from the active nonradiative relaxation and energy transfer between  $\text{Eu}^{3+}/\text{Dy}^{3+}$  ions and host<sup>42,48</sup>. Notably, this error affects little on the values of  $S_a$  and  $S_r$ , as shown in

Figure 4.10(b,c).



## 5. Conclusions

In this work, a series of  $\text{Eu}^{3+}/\text{Dy}^{3+}$  co-doped  $\text{SrWO}_4$  phosphors were prepared by the high-temperature solid-state method. The structural property was studied by the X-Ray diffraction. The emission intensity, fluorescence color, and lifetimes of  $\text{Dy}^{3+}$  (572 nm) and  $\text{Eu}^{3+}$  (615 nm) of the  $\text{SrWO}_4:0.4 \text{ mol\% Eu}^{3+}, 4 \text{ mol\% Dy}^{3+}$  are investigated in the temperature from 11 K to 529 K under the 266 nm excitation. The emission intensity ratio of  $\text{Dy}^{3+}$  and  $\text{Eu}^{3+}$  ions was found to be temperature dependent. The maximum value of  $S_r$  can be reached 1.71%  $\text{K}^{-1}$  at 335 K, being higher than those previously reported material. This work opens a new route to obtain optical thermometry with high sensitivity through using down-conversion fluorescence under ultraviolet excitation.

## **Acknowledgements**

Foremost, I would like to express my gratitude to my supervisor, professor Hyo Jin Seo, for his continuous support, patience, encouragement and immense knowledge that contributed to the completion of thesis. His guidance has helped me a lot during the two years of research and living in South Korea. I would like to extend my sincere thanks to Dr. Peiqing Cai. Thanks to his instructive guidance and comprehensive education during the two years' schooling.

Please allow me to give my grateful thanks to Prof. Xiangfu Wang. Without his consistent and illuminating instruction, this thesis could not have reached its present form.

I would like to express my appreciation to all of my warmhearted lab-mates, Lin Qin, Cuili Chen and Han Cheng, who gave me their kindly help both in my learning and living. I also would like to express my gratitude to my friend Ting Yu, who gave me a lot of help during my life in Korea.

Last but not least, I am grateful to my parents and other relatives, thank you for your support and encouragement during these years.

## References

1. Kim, J.S., Jeon, P.E., Choi, J.C., Park, H.L., Mho, S.I., & Kim, G.C. Warm-white-light emitting diode utilizing a single-phase full-color  $\text{Ba}_3\text{MgSi}_2\text{O}_8:\text{Eu}^{2+}, \text{Mn}^{2+}$  phosphor. *Applied Physics Letters* **84**, 2931-2933 (2004).
2. Ye, S., Xiao, F., Pan, Y.X., Ma, Y.Y., & Zhang, Q.Y. Phosphors in phosphor-converted white light-emitting diodes: Recent advances in materials, techniques and properties. *Materials Science and Engineering: R: Reports* **71**, 1-34 (2010).
3. Xie, R.J., Hirosaki, N., Kimura, N., Sakuma, K., & Mitomo, M. 2-phosphor-converted white light-emitting diodes using oxynitride/nitride phosphors. *Applied physics letters* **90**, 191101 (2007).
4. Kuznetsov, A.S., Nikitin, A., Tikhomirov, V.K., Shestakov, M.V., & Moshchalkov, V.V. Ultraviolet-driven white light generation from oxy-fluoride glass co-doped with  $\text{Tm}^{3+}$ - $\text{Tb}^{3+}$ - $\text{Eu}^{3+}$ . *Applied Physics Letters* **102**, 161916 (2013).
5. Wang, X., Zheng, J., Xuan, Y., & Yan, X. Optical temperature sensing of  $\text{NaYbF}_4: \text{Tm}^{3+} @ \text{SiO}_2$  core-shell micro-particles induced by infrared excitation. *Optics express* **21**, 21596-21606 (2013).
6. Das, S., Reddy, A.A., Babu, S.S., & Prakash, G.V. Controllable white light emission from  $\text{Dy}^{3+}$ - $\text{Eu}^{3+}$  co-doped  $\text{KCaBO}_3$  phosphor. *Journal of materials science* **46**, 7770 (2011).
7. Laguna, M., Nuñez, N.O., Becerro, A.I., & Ocaña, M. Morphology control

of uniform CaMoO<sub>4</sub> microarchitectures and development of white light emitting phosphors by Ln doping (Ln= Dy<sup>3+</sup>, Eu<sup>3+</sup>). CrystEngComm (2017).

8. Hirai, T., & Kawamura, Y. Preparation of Sr<sub>2</sub>CeO<sub>4</sub>: Eu<sup>3+</sup>, Dy<sup>3+</sup> white luminescence phosphor particles and thin films by using an emulsion liquid membrane system. The Journal of Physical Chemistry B **109**, 5569-5573 (2005).

9. Berry, M. T., May, P. S., & Xu, H. Temperature dependence of the Eu<sup>3+</sup> <sup>5</sup>D<sub>0</sub> lifetime in europium tris (2, 2, 6, 6-tetramethyl-3, 5-heptanedionato). The Journal of Physical Chemistry **100**, 9216-9222 (1996).

10. Morgan, J. R., & El-Sayed, M. A. Temperature dependence of the homogeneous linewidth of the <sup>5</sup>D<sub>0</sub>-<sup>7</sup>F<sub>0</sub> transition of Eu<sup>3+</sup> in amorphous hosts at high temperatures. Chemical Physics Letters **84**, 213-216 (1981).

11. Eckert, C., Pflitsch, C., & Atakan, B. Dy<sup>3+</sup>:Al<sub>2</sub>O<sub>3</sub> and (Dy<sup>3+</sup> + Cr<sup>3+</sup>): Al<sub>2</sub>O<sub>3</sub> films for temperature sensor applications derived by thermal CVD and sol-gel techniques. ECS Transactions **25**, 1293-1300 (2009).

12. Zhou, B., Bu, Y. Y., Meng, L., Yan, X. H., & Wang, X. F. Temperature-controlled down-conversion luminescence behavior of Eu<sup>3+</sup>-doped transparent MF<sub>2</sub> (M= Ba, Ca, Sr) glass ceramics. Luminescence. (2016).

13. Dutta, S., & Sharma, S. K. Energy transfer between Dy<sup>3+</sup> and Eu<sup>3+</sup> in Dy<sup>3+</sup>/Eu<sup>3+</sup>-codoped Gd<sub>2</sub>MoO<sub>6</sub>. Journal of Materials Science **51**, 6750-6760 (2016).

14. Liu, Y., Liu, G., Dong, X., Wang, J., & Yu, W. Tunable photoluminescence

and magnetic properties of Dy<sup>3+</sup> and Eu<sup>3+</sup> doped GdVO<sub>4</sub> multifunctional phosphors. *Physical Chemistry Chemical Physics* **17**,26638-26644(2015).

15. Bharat,L.K.,& Yu,J.S. Synthesis and luminescent properties of Eu<sup>3+</sup> activated SrWO<sub>4</sub> nanocrystalline microspheres. *Journal of nanoscience and nanotechnology* **13**,8239-8244(2013).

16. Barros,B.S.,De Lima,A.C.,Da Silva,Z.R.,Melo,D.M.A.,& Alves-Jr,S. Synthesis and photoluminescent behavior of Eu<sup>3+</sup>-doped alkaline-earth tungstates. *Journal of Physics and Chemistry of Solids* **73**,635-640(2012).

17. Neeraj,S.,Kijima,N.,& Cheetham,A.K. Novel red phosphors for solid-state lighting: the system NaM(WO<sub>4</sub>)<sub>2-x</sub>(MoO<sub>4</sub>)<sub>x</sub>:Eu<sup>3+</sup> (M= Gd, Y, Bi). *Chemical Physics Letters* **387**,2-6(2004).

18. Klick,C.C.,& Schulman,J.H. Luminescence in solids. *Solid State Physics* **5**,97-172(1957).

19. Riseberg,L.A.,& Moos,H.W. Multiphonon orbit-lattice relaxation of excited states of rare-earth ions in crystals. *Physical Review* **174**,429(1968).

20. Blasse,G.. On the Eu<sup>3+</sup> Fluorescence of Mixed Metal Oxides. IV. The Photoluminescent Efficiency of Eu<sup>3+</sup>-Activated Oxides. *The Journal of Chemical Physics* **45**,2356-2360(1966).

21. Mota,N.,Ismagilov,I.Z.,Matus,E.V.,Kuznetsov,V.V.,Kerzhentsev,M.A.,Ismagilov,Z.R., Navarro,R.M.,& Fierro,J.L.G. Hydrogen production by autothermal reforming of methane over lanthanum chromites modified with Ru and Sr. *International Journal of Hydrogen Energy*

**41**,19373-19381(2016).

22. Sharma,K.G.,& Singh,N.R. Synthesis and luminescence properties of  $\text{CaMO}_4:\text{Dy}^{3+}$  (M= W, Mo) nanoparticles prepared via an ethylene glycol route. *New Journal of Chemistry* **37**,2784-2791(2013).

23. Singh,B.P.,Singh,J.,& Singh,R.A. Luminescence properties of  $\text{Eu}^{3+}$ -activated  $\text{SrWO}_4$  nanophosphors-concentration and annealing effect. *RSC Advances* **4**,32605-32621(2014).

24. Tozri,A.,Bejar,M.,Dahri,E.,& Hlil,E.K. Structural and magnetic characterisation of the perovskite oxides  $\text{La}_{0.7}\text{Ca}_{0.3-x}\text{Na}_x\text{MnO}_3$ . *Central European Journal of Physics* **7**,89-95(2009).

25. Ahmad,G.,Dickerson,M.B.,Church,B.C.,Cai,Y.,Jones,S.E.,Naik,R.R.,King,J. S.,Summers,C. J.,Kröger,N.,& Sandhage,K.H. Rapid, Room - Temperature Formation of Crystalline Calcium Molybdate Phosphor Microparticles via Peptide - Induced Precipitation. *Advanced Materials* **18**,1759-1763(2006).

26. Li,L.Z.,Yan,B.,Lin,L.X.,& Zhao,Y. Solid state synthesis, microstructure and photoluminescence of  $\text{Eu}^{3+}$  and  $\text{Tb}^{3+}$  activated strontium tungstate. *Journal of Materials Science: Materials in Electronics* **22**,1040-1045(2011).

27. Liu,Y.,Liu,G.,Wang,J.,Dong,X.,& Yu,W. Single-component and warm-white-emitting phosphor  $\text{NaGd}(\text{WO}_4)_2:\text{Tm}^{3+},\text{Dy}^{3+},\text{Eu}^{3+}$ : synthesis, luminescence, energy transfer, and tunable color. *Inorganic chemistry* **53**,11457-11466(2014).

28. Watras,A.,Dereń,P.J.,& Pązik,R. Luminescence properties and determination of optimal RE<sup>3+</sup>(Sm<sup>3+</sup>, Tb<sup>3+</sup> and Dy<sup>3+</sup>) doping levels in the KYP<sub>2</sub>O<sub>7</sub> host lattice obtained by combustion synthesis. *New Journal of Chemistry* **38**,5058-5068(2014).
29. Ju,Z.,Wei,R.,Gao,X.,Liu,W.,& Pang,C. Red phosphor SrWO<sub>4</sub>:Eu<sup>3+</sup> for potential application in white LED. *Optical Materials* **33**,909-913(2011).
30. Lin,J.,Su,Q.,Wang,S.,& Zhang,H. Influence of crystal structure on the luminescence properties of bismuth (III), europium (III) and dysprosium (III) in Y<sub>2</sub>SiO<sub>5</sub>. *Journal of Materials Chemistry* **6**,265-269(1996).
31. Luo,L.,Huang,F.Y.,Dong,G.S.,Wang,Y.H.,Hu,Z.F.,& Chen,J. White Light Emission and Luminescence Dynamics in Eu<sup>3+</sup>/Dy<sup>3+</sup> Codoped ZnO Nanocrystals. *Journal of Nanoscience and Nanotechnology* **16**,619-625(2016).
32. Sudarsan,V.,Van Veggel,F.C.,Herring,R.A.,& Raudsepp,M. Surface Eu<sup>3+</sup> ions are different than “bulk” Eu<sup>3+</sup> ions in crystalline doped LaF<sub>3</sub> nanoparticles. *Journal of Materials Chemistry* **15**,1332-1342(2005).
33. Yang,H.M.,Shi,J.X.,Liang,H.B.,& Gong,M.L. A novel red phosphor Mg<sub>2</sub>GeO<sub>4</sub> doped with Eu<sup>3+</sup> for PDP applications. *Materials Science and Engineering: B* **127**,276-279(2006).
34. Wan,J.,Cheng,L.,Sun,J.,Zhong,H.,Li,X.,Lu,W.,Tian,Y.,Lin,H.,& Chen,B. Energy transfer and colorimetric properties of Eu<sup>3+</sup>/Dy<sup>3+</sup> co-doped Gd<sub>2</sub>(MoO<sub>4</sub>)<sub>3</sub> phosphors. *Journal of Alloys and Compounds* **496**,331-334(2010).

35. Chen,D.,Wang, Y., Yu, Y.,Huang,P.,& Weng,F. Near-infrared quantum cutting in transparent nanostructured glass ceramics. *Optics letters* **33**,1884-1886(2008).
36. Nikolić,M.G.,Antić,Ž.,Ćulubrk,S.,Nedeljković,J.M.,& Dramićanin,M.D. Temperature sensing with  $\text{Eu}^{3+}$  doped  $\text{TiO}_2$  nanoparticles. *Sensors and Actuators B: Chemical* **201**,46-50(2014).
37. Wang,X.,Liu,Q.,Cai,P.,Wang,J.,Qin,L.,Vu,T.,& Seo,H.J. Excitation powder dependent optical temperature behavior of  $\text{Er}^{3+}$  doped transparent  $\text{Sr}_{0.69}\text{La}_{0.31}\text{F}_{2.31}$  glass ceramics. *Optics Express* **24**,17792-17804(2016).
38. Xiao,S.,Yang,X.,Liu,Z.,& Yan,X.H. Up-conversion in  $\text{Er}^{3+}:\text{Y}_2\text{O}_3$  Nanocrystals Pumped at 808 nm. *Journal of applied physics* **96**,1360-1364(2004).
39. Shinn,M.D.,Sibley,W.A.,Drexhage,M.G.,& Brown,R.N. Optical transitions of  $\text{Er}^{3+}$  ions in fluorozirconate glass. *Physical Review B* **27**,6635(1983).
40. Dramićanin,M.D. Sensing temperature via downshifting emissions of lanthanide-doped metal oxides and salts. A review. *Methods and Applications in Fluorescence* **4**,042001(2016).
41. Xu,B.,Cao,X.,Wang,G.,Li,Y.,Wang,Y.,& Su,J. Controlled synthesis and novel luminescence properties of string  $\text{SrWO}_4:\text{Eu}^{3+}$  nanobeans. *Dalton Transactions* **43**,11493-11501(2014).
42. Wang,X.,Liu,Q.,Bu,Y.,Liu,C.S.,Liu,T.,& Yan,X. Optical temperature

- sensing of rare-earth ion doped phosphors. *Rsc Advances* **5**,86219-86236(2015).
43. Cao,Z.,Zhou,S.,Jiang,G.,Chen,Y.,Duan,C.,& Yin,M. Temperature dependent luminescence of Dy<sup>3+</sup> doped BaYF<sub>5</sub> nanoparticles for optical thermometry. *Current Applied Physics* **14**,1067-1071(2014)
44. Lojpur,V.,Ćulubrk,S.,& Dramićanin,M.D. Ratiometric luminescence thermometry with different combinations of emissions from Eu<sup>3+</sup> doped Gd<sub>2</sub>Ti<sub>2</sub>O<sub>7</sub> nanoparticles. *Journal of Luminescence* **169**,534-538(2016).
45. Nikolić,M.G.,Jovanović,D.J.,& Dramićanin,M.D. Temperature dependence of emission and lifetime in Eu<sup>3+</sup>-and Dy<sup>3+</sup>-doped GdVO<sub>4</sub>. *Applied optics* **52**,1716-1724(2013).
46. Meert,K.W.,Morozov,V.A.,Abakumov,A.M.,Hadermann,J.,Poelman,D., & Smet,P.F. Energy transfer in Eu<sup>3+</sup> doped scheelites: use as thermographic phosphor. *Optics express* **22**,A961-A972(2014).
47. Boruc,Z.,Kaczkan,M.,Fetlinski,B.,Turczynski,S.,& Malinowski,M. Blue emissions in Dy<sup>3+</sup> doped Y<sub>4</sub>Al<sub>2</sub>O<sub>9</sub> crystals for temperature sensing. *Optics letters* **37**,5214-5216(2012).
48. Wade,S.A.,Collins,S.F.,& Baxter,G.W. Fluorescence intensity ratio technique for optical fiber point temperature sensing. *Journal of Applied physics* **94**,4743-4756(2003).